PERMEABILITY MEASUREMENT FOR LARGE ROCK FRACTURE USING RUBBER-CONFINING PRESSURE VESSEL

N. WATANABE, N. HIRANO & N. TSUCHIYA

Graduate School of Environmental Studies, Tohoku University, Sendai, Japan

SUMMARY – The newly developed rubber-confining pressure vessel (R-CPV) enabled simple and easy permeability measurement for large fractures under high confining pressure. The permeability measurements for granite samples including single tensile fractures of 100 x 150mm with various lateral displacement along fracture surfaces were performed under the confining pressures up to 100MPa using the R-CPV. For fractures without lateral displacement, the permeability decreased with increasing confining pressure until 40-50MPa, beyond which the permeability decreased gently or became constant. For fractures with lateral displacement, significant increase of permeability occurred even for lateral displacement as small as 1mm. The permeability, however, decreased with increasing confining pressure, and a rapid decrease occurred at 80MPa for 1mm displacement. For the fracture with sufficiently larger lateral displacement -more than 3mm, obvious decrease of permeability did not occur as increasing confining pressure and remained large even under high confining pressure.)

1 . INTRODUCTION

Transport phenomena of fluids in rock fractures are greatly influenced by fracture apertures and their spatial distribution (Brown, 1987; van Genabeek and Rothman, 1999) due to roughness of fractal fracture surfaces (Brown and Scholtz, 1985; Power *et al*., 1988; Tsuchiya and Nakatsuka, 1995, 1996). Fracture apertures and their distribution depend on normal and sheer stress (Yeo *et al*.1998; Chen *et al*, 2000) and a variety of rocks (Sausse, 2002) and changed due to fluid-rock interactions (Watanabe and Tsuchiya, 2003).

To understand transport phenomena such as fluid flow properties and permeability under lithospheric stress, it is necessary to measure fracture permeability considering roughness and stress. Numerical simulations are also needed (Pyrak-Nolte and Morris, 2000; Matsuki *et al*., 2001; Sausse, 2002). In addition, experimental results that satisfy the conditions of the simulations are needed for improvement of the simulations. Therefore, the experiments close to natural conditions, i.e. experiments using the samples including fractures of as large area as possible under the stresses, such as their permeability reflects two dimensional fluid flow, are needed.

In the previous studies, methods for measuring fracture permeability under normal stress have been flow tests for orthogonal or cylindrical samples, including horizontal fracture under uni-axial compressive load using a pressing machine, or the flow tests for a cylindrical sample, including a fracture parallel to its axis under confining pressure by fluid pressure. In the first case, a pressing machine of higher capacity is needed as increasing normal stress or fracture size means that the normal stress is controlled directly by the capacity of the pressing machine and area of fracture. In the latter case, problems arise from high pressures on seals which are used to keep the fluid under pressure and to separate confined fluid from the fluid for permeability measurement. Therefore, a new confining pressure vessel for simple and easy permeability measurement for a sample including large fracture under high confining pressure have been developed. The new confining pressure vessel is called the rubber-confining pressure vessel (R-CPV).

In this paper, we describe the R-CPV and the results of permeability measurements for granite samples including large tensile fracture of 100 x 150mm with various lateral displacements along fracture surfaces under confining pressure up to 100MPa using the R-CPV.

2. METHODS

2. 1 Sample preparation

The Inada granite quarried in Ibaraki prefecture, Japan was used in this study. The main minerals of the Inada granite are quartz, orthoclase, plagioclase and biotite, and average grain sizes of these minerals are 3.3mm, 3.0mm, 2.5mm and 0.9mm respectively. The matrix permeability is 6.7 x 10^{-19} m^2. The mechanical and physical properties of the Inada granite are shown in Table 1.

Table 1. Mechanical and physical properties of the Inada granite[a] (Matsuki *et al*., 2001).

Uniaxial compressive strength [MPa]	Uniaxial tensile strength [MPa]	Yang's modulus[b] [GPa]	Poisson's ratio [-]	Specific gravity [-]	Porosity [%]
163	5.82	71.3	0.2	2.64	0.5

a Mchanical properties were measured by applying the load perpendicular to rift plane.
b Tangential Yang's modulus at 50% of uniaxial compressive strength.

The procedure of sample preparation is shown in Fig. 1. First, a 200mm cubic Inada granite block is notched using a disc cutter (Fig. 1a). A single tensile fracture is created in the block using a wedge (Fig. 1b). The bock is fixed with an arbitrary lateral displacement along fracture surfaces using acrylic plates, which are the same thickness as the displacement (Fig.1c). Finally, the block is turned into a cylinder 100mm in diameter and 150mm in length, a fracture parallel to its axis is obtained (Fig.1d). The apparent fracture area is 100 x 150mm. The directions of both the fracture propagation and the lateral displacement are parallel to the radius of samples. In this study, seven samples were prepared. Three of these samples were given no lateral displacement (NC01, NC02 and NC03) and the remains were given lateral displacement of 1mm (NC05), 3mm (NC07), 5mm (NC06) and 10mm (NC09) respectively.

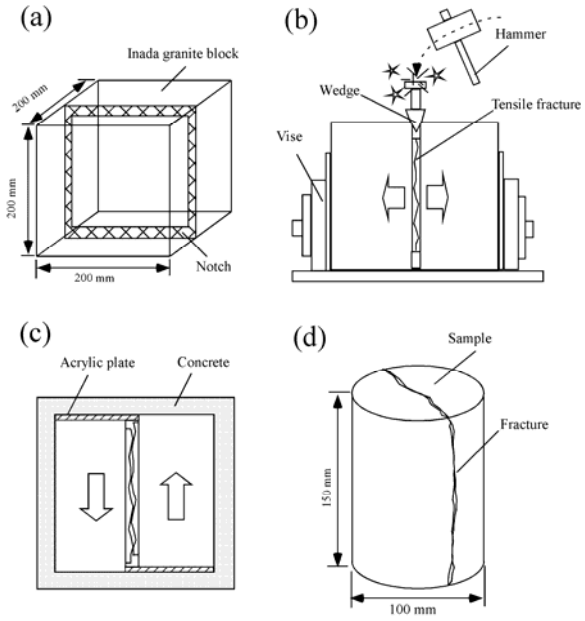

Fig. 1. Preparation of experimental sample. (a) Notch the granite block, (b) Creation of single tensile fracture using an edge, (c) Lateral displacement along fracture using acrylic plates, and (d) Shaping of the cylindrical shape 100mm in diameter and 150mm in length.

The fractal dimension and RMS of fracture surfaces were evaluated in the direction parallel to the axis and radius, respectively. The spectral method was used in this study (Power and Durham, 1997). The relationship between power spectral density and spatial frequency on log-log diagram was linear at range of about 0.02-0.4mm^{-1}. The summary of fractal dimension and RMS obtained for each sample is shown in Table 2. ”Lower” and ”Upper” indicate two fracture surfaces of a sample for convenience, and “Radius” and ”Axis” indicate the directions of the calculation. The fractal dimension in the direction parallel to axis of upper surface of NC01 was not determined since the power spectral density function fluctuated considerably, possibly as a consequence of sample preparation.

The anisotropic fractal dimension was observed for several surfaces. The fractal dimension in the direction parallel to radius was larger than that in the direction parallel to the axis. The direction parallel to radius corresponds to the direction of fracture propagation. Consequently, this anisotropy could be related with the direction of fracture propagation. Although the differences of fractal dimension between the upper and lower surfaces were also observed, these differences could be caused by separation of small particles from the surfaces since these differences are smaller than those of between the directions. For the tensile fractures created in this study, the average of fractal dimension and RMS were 1.49 and 1.50 respectively. This value of fractal dimension is the almost same compared with the fractal dimension evaluated for the fractures created by hydraulic fracturing and natural fractures (Brown and Scholtz, 1985).

Table 2. Fractal dimension, D, and RMS of fracture surfaces.

Sample	Surface	D (Radius) [-]	D (Axis) [-]	RMS (Radius) [mm]	RMS (Axis) [mm]
NC01	Lower	1.52	1.41	1.57	2.09
	Upper	1.53	N. D.*	1.55	2.17
NC02	Lower	1.50	1.43	1.14	1.75
	Upper	1.52	1.42	1.08	1.67
NC03	Lower	1.48	1.44	1.12	2.18
	Upper	1.50	1.55	1.16	2.14
NC05	Lower	1.54	1.43	1.11	1.51
	Upper	1.51	1.42	1.12	1.50
NC06	Lower	1.59	1.53	1.29	1.22
	Upper	1.45	1.50	1.35	1.21
NC09	Lower	1.44	1.42	1.12	2.01
	Upper	1.40	1.53	1.19	1.95

* Not determined

2. 2 Apparatus and procedure

In this study, the rubber-confining pressure vessel (R-CPV) developed for fracture permeability measurements were used (Fig. 2). The main components of the R-CPV are an outer cylinder, an inner cylinder, a butadiene rubber for pressure medium, two hollow pistons for compressing the rubber and two outer pistons.

A cylindrical sample, which is 100mm in diameter and 150mm in length, surrounded by the rubber is put in the inner cylinder, and two hollow pistons are inserted into the inner cylinder. The internal and external diameter of these hollow pistons are the same as the diameter of the sample and the internal diameter of the inner cylinder respectively, so that these two hollow pistons can compress only the

rubber. In addition, the blocks, made of natural rubber and aluminum, are set above and below the samples respectively to prevent the sample from breaking due to the axial tensile stress caused by confining pressure. Then these parts are inserted in the outer cylinder, and two outer pistons with water pipes are inserted in the outer cylinder.

The mechanism of applying confining pressure on the sample is outlined below. It is known that the rubber elasticity resembles the elasticity of compressed gases. This means that when the sealed rubber is compressed with the hollow piston, the isotropic pressure, which is the same as pressure acting on the contact area between the rubber and hollow piston, is generated as the Pascal's principle and acts as confining pressure on the sample. The confining pressure depends on compressive load and cross sectional area of the rubber (i.e. hollow pistons). The R-CPV enables a large sample to be subjected to high confining pressure on a pressing machine of low capacity. This has the advantage that consideration of the seal is not necessary because no fluid for confining pressure is used. Additionally, the normal stress, which is same as confining pressure, acts on the fracture when the fracture is parallel to the axis of sample.

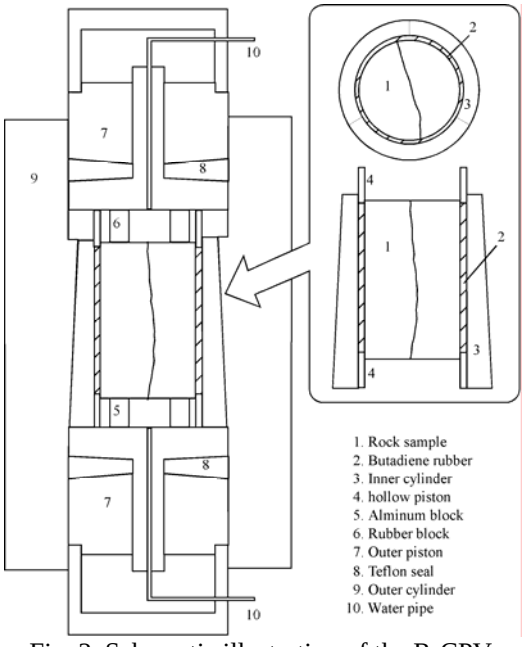

Fig. 2. Schematic illustration of the R-CPV.

The experimental system for permeability measurements using the R-CPV is shown in Fig. 3. The R-CPV is placed in the pressing machine of maximum load of 25t. Controlling the load controls the confining pressure, and its range is from 10 to 100MPa for the capacity of this pressing machine. The water in a tank is pumped into the R-CPV through the lower outer piston, and flows through the fracture of the sample, and then flows out through upper outer piston. The water pipes connected to the outer pistons are branched off and connected to a differential pressure gauge to measure the hydraulic pressure drop occurring in the fracture.

The experiments were performed using the following procedure and 20°C purified water.

1. Set the sample in R-CPV and adjust confining pressure to 10MPa.
2. Keep pumping water into R-CPV for twelve hours in order to saturate the fracture with water.
3. Measure flow rate and differential pressure in steady state at several conditions.
4. Increase confining pressure.
5. Repeat step 3 and step 4.

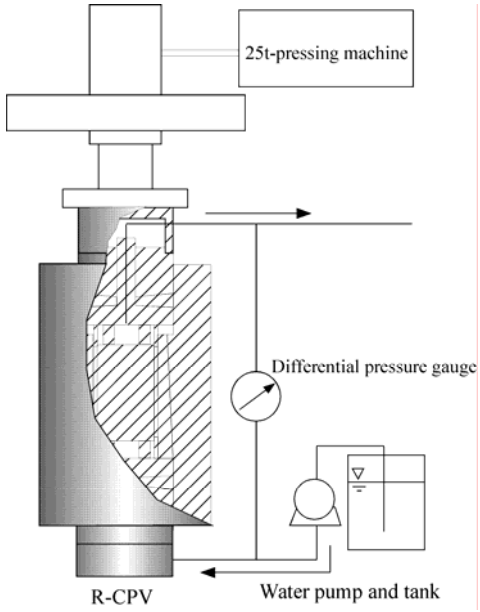

Fig. 3. Schematic illustration of experimental system.

3. RESULTS

The flow rate and differential pressure under different confining pressure for each sample were measured. The result for NC01 is shown in Fig. 4 as a representative result. The solid lines in the diagram are linear regressions of the relationship between flow rate and differential pressure by the least-square method. This indicates that the relationship flow rate and differential pressure is well approximated by a linear relationship for all confining pressures. These linear relationships are observed for all other samples as well.

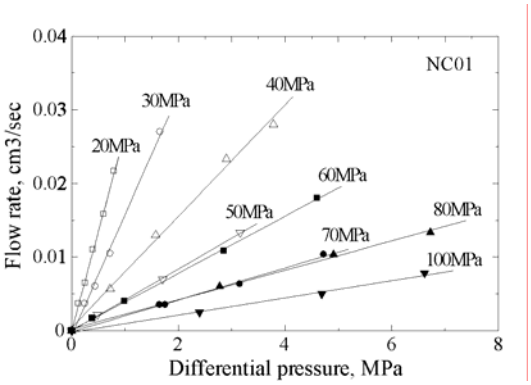

Fig. 4. Relationship between flow rate and differential pressure under various confining pressures for NC01.

Consequently, the fluid flow through the fracture follows the Darcy's law at the range of flow rate in these experiments. The slope of solid lines corresponds to permeability of samples, so that the fracture permeability can be represented as follows.

According to Darcy's law, fluid flow through a porous medium can be expressed as

$$Q = -\frac{kA}{\mu}\frac{\Delta P}{L}, \qquad (1)$$

where Q is flow rate through the sample, k is permeability of the sample, A is the cross-sectional flow area of the sample, ΔP is pressure drop through the sample, μ is fluid viscosity and L is sample length. As much as the granite matrix has little or no permeability, the permeability of samples measured in this study mainly results from the fracture. As such, k can be considered as the permeability of the fracture if the cross-sectional area of fracture substitutes the flow area. Assuming that a fracture has a unique width of e_h, which is defined as hydraulic aperture of fracture, the permeability of fracture can be given by the parallel plate model as

$$k = \frac{e_h^2}{12}. \qquad (2)$$

Combining equations (1) and (2) and denoting fracture-sectional area as $A=de_h$, the hydraulic aperture of fracture can be expressed as

$$e_h = \left(-\frac{12\mu QL}{d\Delta P}\right)^{1/3} \qquad (3)$$

where d is fracture length orthogonal to the no-flow boundary (Chen *et al*, 2000).

The relationships between permeability and confining pressure for three samples without lateral displacement along fracture surfaces are shown in Fig. 4. The permeability ranged between about 0.5-8x10^{-12} m^2 and the permeability decreased significantly at 40-50MPa for all three samples. While the permeability decreased with increasing confining pressure when confining pressures were lower than 40-50MPa, the permeability decreased gently or became constant when confining pressures were higher than 40-50MPa.

Although the permeability and the behavior of decrease were almost the same in all three samples, the permeability under the same confining pressure differed among the three samples especially when confining pressure was lower than 40-50MPa. For instance, the permeability at 20MPa was large in NC01, NC02 and NC03. The differences, however, became smaller gradually under confining pressure higher than 40-50MPa, and the permeability of each sample tended to converge at 100MPa.

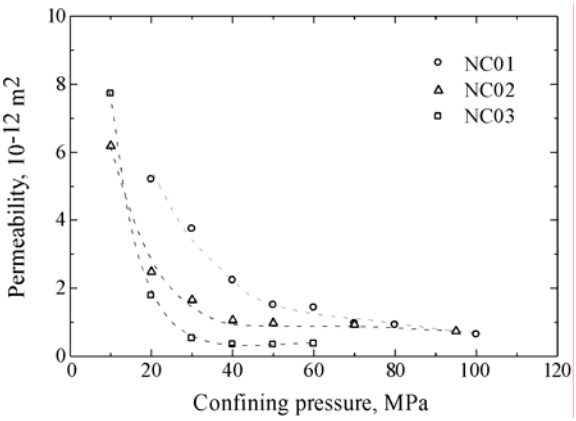

Fig. 5. Relationship between permeability and confining pressure for the samples without lateral displacement.

The relationships between the permeability and confining pressure for the samples with lateral displacement of 1, 3, 5 and 10mm are shown in Fig. 5. The permeability ranged between about 0.5-4x$10^{-9}$$m^2$ for all lateral displacement except for the permeability at 80MPa and 100MPa of the sample with 1mm lateral displacement. These values were three-orders larger than those of the samples without lateral displacement.

The behavior of permeability with increase of confining pressure differed significantly between the sample with 1mm lateral displacement and the others. For the sample with lateral displacement of 1mm, the permeability decreased continuously as confining pressure increased from 10 to 70MPa and then decreased abruptly at 80MPa. For the samples with lateral displacement more than 3mm, the permeability was reduced only at 20-30MPa, and the obvious decrease was not observed under higher confining pressure. Additionally it was observed that the permeability became larger with increasing lateral displacement.

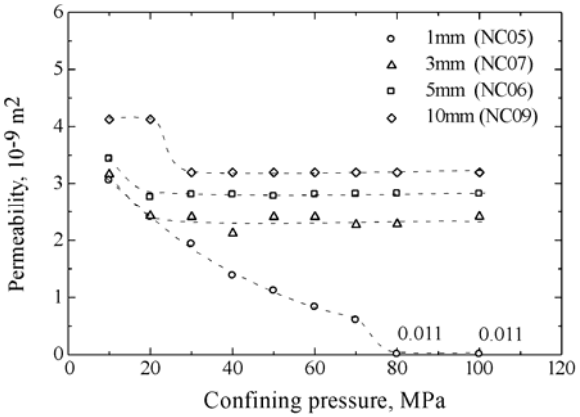

Fig. 6. Relationship between permeability and confining pressure for the samples with lateral displacement.

4. DISCUSSION

For the samples without lateral displacement, the significant decrease in permeability was observed at 40-50MPa. Taking account of no lateral displacement along fracture surfaces, relatively large contact area can exist since opposite fracture surfaces are well mated. The concentration of normal load on the fractures, which crushes the asperities of fracture surfaces, cannot occur. In fact, the abrupt decreases, which could be caused by such crushing asperities, have not been observed. Consequently, both the decrease of permeability due to the decrease of fracture aperture and new contact points due to elastic deformation of the fracture surfaces can occur as increasing confining pressure until a certain magnitude. Beyond the certain magnitude the decrease of permeability become less significant due to dispersion of normal load because of the relative large contact area compared to initial condition. In this study, this happened at 40-50MPa.

Although the behavior of the decrease of permeability was similar for the all three samples, the permeability differs among the samples below 40-50MPa. These differences could be caused by the different fracture surface roughness of individual samples due to differences of amount of particles separated from surfaces, degree of damage or other factors during the sample preparation process.

For the samples with lateral displacement, the permeability was three-orders larger compared with the samples without lateral displacement even with small displacement of 1mm and became larger as increasing lateral displacement. This results from increased fracture aperture due to lateral displacement (Yeo *et al*.1998；Chen *et al*, 2000).

For the sample with lateral displacement of 1mm, the permeability decreased continuously as the confining pressure increased from 10 to 70MPa and deceased abruptly at 80MPa. These results indicate that continuous decrease of permeability occurred due to elastic deformation of fracture surfaces until 70MPa and discontinuous abrupt decrease occurred at 80MPa due to crossing contact points. It is noted that the abrupt decrease can occur for the fracture with such a small lateral displacement.

For the samples with larger lateral displacement-more than 3mm, the obvious decrease of permeability at increased confining pressure was not observed. Contact area and stiffness of fracture become smaller with increasing lateral displacement in general. The permeability, however, was reduced discontinuously only at 20-30MPa. This discontinuous decrease could occur due to crushing contact points at 20-30MPa, beyond which the obvious decrease of permeability couldn't be observed because of the remained relative large aperture.

5. CONCLUSIONS

In this study, tensile fractures were created artificially in the Inada granite using a wedge, and the samples including a single fracture of 100 x 150mm with lateral displacement of 0, 1, 3, 5 and 10mm along fracture surfaces were prepared. Permeability measurements for these samples were performed under confining pressure from 10 to 100MPa using the R-CPV. The main conclusions are as follows.

The R-CPV enables simple and easy permeability measurements for a sample including large fracture under high confining pressure.

For a fracture without lateral displacement, permeability decreased with increasing confining pressure until a certain confining pressure, 40-50MPa in this study, beyond which permeability decreased gently or become constant.

For a fracture with lateral displacement, significant increase of permeability can occur even with lateral displacements as small as 1mm. The permeability, however, decreased with increasing confining pressure, and abrupt decrease can occur at high confining pressure, 80MPa in this study, with such a small displacement.

For the fracture with sufficiently large lateral displacement, for instance 3mm in this study, obvious decrease of permeability does not occur as increasing confining pressure and remains large even under high confining pressure.

6. REFERENCES

Brown, S. R. (1987) Fluid flow through rock joints: The effect of surface roughness. *Journal of Geophysical Research*, **vol. 92**, pp. 1337-1347.

Brown, S. R., Scholtz, C. H. (1985) Broad bandwidth

study of the topography of natural rock surfaces, *Journal of Geophysical Research*, **vol. 90**, pp. 2575-12582.

Chen, Z., Narayan, S. P., Yang, Z., Rahman, S. S. (2000) An experimental investigation of hydraulic behavior of fractures and joints in granitic rock. *International Journal of Rock Mechanics and Mining Sciences*, **vol. 37**, pp. 1061-1071.

Matsuki, K., Wang, E. Q., Sakaguchi, K., Okumura, K. (2001) Time-dependent closer of a fracture with rough surface under constant normal stress. *International Journal of Rock Mechanics and Mining Sciences*, **vol. 38**, pp. 607-619.

Power, W. L., Durham, W. B. (1997) Topography of natural and artificial fractures in granitic rocks: Implication for studies of rock friction and fluid migration. *International Journal of Rock Mechanics and Mining Sciences*, **vol. 34**, pp. 979-989 .

Power, W. L., Tullis, T. E., Weeks, J. D. (1988) Roughness and wear during brittle faulting. *Journal of Geophysical Research*, **vol. 93**, pp. 15268-15278.

Pyrak-Nolte, L. J., Morris, J. P. (2000) Single fracture under normal stress: The relation ship between fracture specific stiffness and fluid flow. *International Journal of Rock Mechanics and Mining Sciences*, **vol. 37**, pp. 245-262.

Sausse, J. (2002) Hydromechanical properties and alteration of natural fracture surfaces in the Soultz granite (Bas-Rhin, France). *Tectonophysics*, **vol. 348**, pp. 169-185.

Tsuchiya, N. and Nakatsuka, K. (1995) Fractal Analysis and Modeling of a Two-dimensional Fracture Network in a Geothermal Reservoir. *Geothermal Resources Council Transactions*, **vol. 19**, pp. 547-552

Tsuchiya, N. and Nakatsuka, K. (1999) A Two-dimensional Mono-fractal Approach to Natural Fracture Networks in Rocks. *Geothermal Science & Technology*, **vol.6**, pp. 63-82.

van Genabeek, O., Rothman, D. H. (1999) Critical behavior in flow through a rough-walled channel. *Physics Letters A*, **vol. 255**, pp. 31-36.

Watanabe, N. and Tsuchiya N. (2003) Experimental and Numerical Analysis of Hydrothermal Channel Flow Through a Tensile Fracture in Granite. *Geothermal Resource Council Transactions*, **vol. 27**, pp. 743-746.

Yeo, I. W., De Freitas, M. H., Zimmerman, R. W. (1998) Effect of shear displacement on the aperture and permeability of a rock fracture. *International Journal of Rock Mechanics and Mining Sciences*, **vol. 35**, no. 8, pp. 1051-1070.